This is the Pre-Published Version.

This document is the Accepted Manuscript version of a Published Work that appeared in final form in Inorganic Chemistry, copyright © American Chemical Society after peer review and technical editing by the publisher. To access the final edited and published work see https://doi.org/10.1021/acs.inorgchem.7b00683.

"Energy selection channels" for high performance electrolyte: anion-Frenkel defect pair as dominant source for O ion conductions in pyrochlore type lanthanide hafnium oxides SOFC

Mingzi Sun and Bolong Huang*

Department of Applied Biology and Chemical Technology, The Hong Kong Polytechnic University, Hung Hom, Kowloon, Hong Kong SAR, China

*Email: bhuang@polyu.edu.hk

Abstract

The excellent ion conductivities of pyrochlore-type materials are believed to be based on oxygen anion transportations caused by the intrinsic defects, in which the anion Frenkel (a-Fr) pair (V_O+I_O) defect is the most stable one that lacks detailed study. The partially disordered pyrochlore with formation of the a-Fr pair defect will result more disorder in local pyrochlore structure and increase number of possible migration paths for oxygen anions, which could further improve the ion conductivities of materials. Hence, we studied the formation of a-Fr defect pairs in $La_2Hf_2O_7$ as a representative pyrochlore structure by density functional theory calculations (DFT). Three types of defect migration sites have been discovered with the ability to incorporate interstitial oxygen atoms from 48f sites and form a-Fr defect pairs (I_O+$V_{O\,(48f)}$). Besides the most stable vacant 8a sites with lowest defect formation energy of 3.49 eV/pair, two other novel migration sites have been firstly reported with ability to form a-Fr pair defect with formation energies of 6.53, 8.49 eV/pair, respectively. These two new types of migration path, as intermediate sites, could construct a diffuse channel with vacant 8a site for interstitial oxygen anions diffusion in the lattice and significantly decrease the distance and barrier of each jump for oxygen atoms. In contrast with the oxygen interstitial defects, the formation of a-Fr pair defect shows higher priority because of much lower formation energies. Since oxygen anions could be easier to generate and diffuse in the pyrochlore structure, the a-Fr pair defect can be explained as the origin of excellent ion conductivities of pyrochlore materials. This work provides a detailed understanding of relationship between intrinsic defects and electronic properties, which enable us to predict electronic properties of other pyrochlore-type materials in the future study.

Introduction

Nowadays, wider promoted application range of SOFC, higher thermal stability of ion conductivity, longer cyclability, and lower cost with flexible distribution in power plants are increasingly needed. This indeed serves as demands for pollutant-free renewable energy and materials engineering rapidly expand in next generation of energy renovation. Solid oxide fuel cells (SOFCs) have become the most potential power supply technology with high efficiency and low pollution, which draw a lot of attention of scientists[1-4]. It works in power plant presents a rather higher efficiency (40 ~ 60%), which does not necessarily follow the Carnot-Cycle principles. Most reported SOFC materials usually operate at extreme high temperature (above 800 °C) to ensure the high conversion of fuels and ion conductivity of electrolyte. SOFCs consist three main parts, which are an electrolyte to transport oxide ions to electrode and two electrodes (a cathode and an anode). The chemical reactions occurred on electrodes are shown in Figure 1. For present commercial use, the most widely electrolyte of SOFCs is yttria-stabilized zirconia (YSZ), which shows good compatibility with most electrode materials and relative high ion conductivity[5,6]. However, the high operation temperature of SOFCs will bring some disadvantages such as long-term stability of electrolyte and the formation of insulting layer between electrolyte and electrode[7,8]. Therefore, searching for novel electrolyte materials has become the goal of many researches to satisfy the higher requirements for future SOFCs.

Zr-based oxides have become research interest in many fields due to their wide applications in catalyst[9,10], fuel cell electrolyte[7,11], gate dielectric[12] and thermal coating materials[13], and the synthetization of these functional Zr-based material[14,15] are also attracting lots of attention. Among Zr-based oxides, pyrochlore structure materials with formula $A_2B_2O_7$ as $Ln_2Zr_2O_7$ (Ln^{3+} = lanthanide ions) have been investigated a lot as potential electrolyte materials for SOFCs[16-18]. Chemical substitutions or processing could assist the formation of defects as vacancies and structural disorder and further significantly affect properties of these materials. Solomon *et al.*[16] have systematically investigated $Ln_2Zr_2O_7$ compounds in structure, optical properties and ion conductivities through spectroscopic and diffraction methods. This system showed ion conductivity at order of 10^{-2} S/m at 750 °C. The highest ion conductivity of this system has been reported as $Eu_2Zr_2O_7$ at 1000 °C about 2.0 S/m by work of Yamamura *et al.*[18]. Through doping at A site and solid solution can improve ion conductivity of $Ln_2Zr_2O_7$ significantly, but the value is still below conductivity of YSZ that limit their applications in SOFCs. Since Hf atom has close radius with Zr atom, lanthnoid hafnates ($Ln_2Hf_2O_7$) are also pyrochlore structure sharing similar properties, which are also considered as potential electrolytes in SOFCs. In work of Blanchard *et al.*[19], they demonstrated that only when Ln atom radius is larger than Tb, pyrochlore structure would be favoured by spectrum methods. Karthik *et al.*[20] also confirmed this conclusion through neutron diffraction and found that when Ln = La-Nd, the diffractions reflect characteristic satellite pattern of pyrochlore superlattice. $Ln_2Hf_2O_7$ has received considerable attention in other applications including thermal barrier coatings (TBCs)[21], ceramic scintillators[22,23], semiconductors[24,25] and materials to immobilize nuclear waste[26,27]. Most of these applications depend on the great tolerance of pyrochlore structure and the mobility of anion ions in pyrochlore structure.

The relationship between ion conductivities and intrinsic defects of pyrochlore has been studied a lot[28-31]. In the work of Burggraaf *et al.*[28], they demonstrated that the increment in ion conductivity of pyrochlore based on a preferential diffusion path constructed through cation tetrahedral around 48f sites. They also introduced models of considering ionic conductivity as an ensemble of single jumps with the activation enthalpy ΔH reflecting the barrier energy. Later they used calculation method to prove that an oxygen a-Fr pair defect consisting a vacant 48f site and an interstitial oxygen anions at 8*a* site (I_O+$V_{O(48f)}$) was the most stable anion defect in pyrochlore[29]. Some other works also related the ion conductivities with disorder in the lattice[30-32]. However, there lacks

detailed study of the relationship between ion conductivity and intrinsic defect structure in $Ln_2Hf_2O_7$. By comprehending the relationship between the migration mechanism of oxygen anions and ion conductivity, we can apply this simulation model to other similar pyrochlore-type compounds to predict their electronic properties and applications in SOFCs more precisely.

For many cases of novel materials, the experiment data are not available yet or the results are under dispute. DFT based on first principles have become a powerful and efficient method to explore and predict properties of materials (i.e. pyrochlore-type materials[33-36]). Here, through the DFT method, we would investigate the energetic and electronic properties of $Ln_2Hf_2O_7$. Considering the complex unit cell with 88 atoms of $Ln_2Hf_2O_7$, we choose $La_2Hf_2O_7$ as a representative in this work to explore the oxygen atom transport routes and defect formation energies. The aim of this work is to understand the formation process and energies of a-Fr pair defects. Therefore, we will construct quantities of simulation models at different sites with various migration distance to explore the detailed cause of ion conductivity of pyrochlore $La_2Hf_2O_7$.

Crystal Structure

Based on former experiment results of $La_2Hf_2O_7$ crystal structure given by Subramanian *et al.* and Sleight[37,38], a basic cubic crystal with symmetry group of *Fd-3m* comes with a lattice parameter of 10.770 Å (As Figure 2). La atoms will occupy 16d site (1/8, 1/8, 1/8) with Hf atoms at 16c site (1/8, 1/8, 5/8). Oxygen atoms have two non-equivalent positions, that O1 will be at 8b site (0, 0, 0) and O2 will be at 48f site (0.302, 0, 0). In this phase, La has 8-fold coordinated sites, Hf has 6-fold sites and O has 4-fold sites. A complex unit cell with 88 atoms of $La_2Hf_2O_7$ will be used to operate the geometry optimization and further defect formation energy calculations.

Calculation Setup

All the calculations choose the total energy density functional pseudopotential method. The Broyden-Fletcher-Goldfarb-Shannon (BFGS) algorithm will be used through bulk and defect calculations. For bulk properties of $La_2Hf_2O_7$, ultrafine quality is chosen with a plane-wave cutoff energy of 750 eV. A 2×2×2 Monkhost-Pack (MP) k-point mesh will be used, which converged the total energy within 5.0×10^{-6} eV/atom, maximum ionic Hellmann–Feynman force within 0.01 eV/Å and maximum ionic displacement within 5.0×10^{-4} Å.

In our work, the geometry relaxation of the lattice was performed at PBE+U in DFT through CASTEP codes [ref 0], which has been proved that is reliable on many f-orbital based oxides [ref1]. To improve the accuracy of the results of electronic properties, we introduce the recently developed method on ab-initio determination of Hubbard U parameters to carefully avoid extra spurious error from orbital self-interactions [ref 2, 3, 4, 5, 6, 7, 8].

We choose different orbitals projectors for different atoms to represent their valence states. For instance, La with (4f, 5s, 5p, 5d, 6s), Hf with (5s, 5p, 5d, 6s) states and O with (2s, 2p) states have been chosen for pseudopotential generation, respectively. The DFT+U method that developed by Anisimov-type rotational invariant scheme [ref 9]. Note, we also applied the self-consistently determined Hubbard U potentials on the O-2p orbitals to reduce the influence of localized hole states produced by various anion O sites [ref 10, 11, 12, 13, 14, 15, 16, 17]. The OPIUM code in the Kleinman–Bylander form of norm-conserving pseudopotential [Ref 18] with the RRKJ method are chosen [Ref 19] to minimize the systematic error, and to optimize the basis sets and the ionic minimization of the pseudopotentials. The norm-conserving pseudopotentials is chosen because it can reproduce the all-electron behavior for outter shell valence electrons with |**S-matrix**|=1 compared to ultrasoft pseudopotentials [ref 20, 21]. The non-linear partial core correction has been used for minimizing the systematic error due to the atomic core-valence electron densities overlaps

[ref 22], which can accurately describe mix-valence effect of the heavy La^{3+} ion, as well as the strongly localized states induced by 2p orbitals of O.

In the electronic minimization process, to prevent the charge-spin out-sync sloshing effect and guarantee the electronic minimization and convergence, the ensemble DFT (EDFT) method of Marzari et al is used for solving Kohn-Sham equation [ref 23]. We further select the Baldereschi special k-point (¼, ¼, ¼) in the simple cubic 2×2×2 supercell for fast convergence in energy. This converges the total energy to under $5.0x10^{-7}$eV per atom [ref 24].

With our self-consistent determination process [ref 2, 3, 4, 5, 6, 7, 8], as shown in Figure 3, the Hubbard U parameters are decided to be 2.24 eV for 4f-orbitals of La sites and 5.27 eV for 5d-orbitals of Hf-sites. The O-sites within pyrochlore $La_2Hf_2O_7$ have two non-equivalent position and the Hubbard U parameters of 2p-orbitals of O-sites have been determined as 4.93 and 4.83 eV, respectively.

Results and Discussion

Equilibrium Crystal Structure Properties

The experimental lattice parameters and the internal structure parameters are used to construct the original pyrochlore conventional cell model for $La_2Hf_2O_7$ to operate the geometry optimization at constant volume. The initial parameters of the model and parameters after geometry optimization are shown in Table 1 with former calculations and experimental results. As can be seen from the table, the result of lattice constant shows 3.0-3.3% mismatch with the actual experimental data when GGA is used to operate the geometry optimization. This result has significant improvement when operating optimization with corrected GGA+U method. The calculation shows excellent agreement with the actual data from experimental results: the lattice constant has only 0.8-1% mismatch with the experimental data. Moreover, the interatomic distance results are shown in the table, which supports the experimental data as well.

Electronic Properties

By using photoconductivity spectrum, Seguini *et al.*[18] have demonstrated that the bandgap of $La_2Hf_2O_7$ is 5.6 ± 0.1 eV at amorphous phase. Terki *et al.*[33] used DFT+LAPW method implemented in WIEN2K codes to examine $La_2Hf_2O_7$ with result of a 3.34 eV direct bandgap, which has been much underestimated compare to experimental result. The main hurdle of DFT calculation is the underestimation of bandgap when calculating the formation energies or charge transfer levels of defects. Due to the huge difference with experimental data, the GGA+U method has operated to correct the huge mismatch in band structure, which indicates a much more accurate result with a direct bandgap of 5.880 eV (Figure 4). This result is much remarkably close to the experiment data that prove the validity of correctness on this calculation method. In Figure 4, we can also indicate the orbital composition of $La_2Hf_2O_7$ in TDOS (Total density of states). Below the valence band maximum (VBM) (E_V = 0 eV), contributions are mainly from O atoms while the Hf and La atoms mainly contribute to the conduction band (CB). The top of VB consists of levels mainly from O-2p orbitals. The bottom of the CB (or conduction band minimum, CBM) is mainly occupied by the Hf-5d orbitals, while overall in the lower conduction band, La-4f and Hf-5d orbitals are the main contribution. The La-4f vacant level shows a sharp high peak at range of 5-8 eV, which is overlapping with Hf-5d orbitals.

Anion Frenkel Pair Defect

The ion conductivities of pyrochlore-type materials are believed that mostly based on the transportation of oxygen anions in the structure. Dijk *et al.*[39] introduced a model of considering ion

conductivity as single jumps of oxygen atoms from original positions with the activation enthalpy reflecting the barrier energy. They suggested that 48f→48f jumps would be energetically favourable pathway for oxygen anions. However, in the work of Wilde *et al.*[32], they calculated formation energies of different kinds of defects in pyrochlore-type compounds. The formation energy of a-Fr pair defects varied from 3.2-5.3 eV/pair that was much lower than 48f vacancy and 8a vacancy. Hence, we will concentrate on a-Fr pair defect pair of $La_2Hf_2O_7$ as a representative of pyrochlore-type structures in our work. An oxygen a-Fr pair defect represents that an oxygen atom escapes from its original position, leaving a vacancy, to an interstitial site after absorbing enough energy. The oxygen vacancy (V_O) and the interstitial (I_O) pair will be called a-Fr pair defect. To construct simulation models, we artificially move one oxygen atom from 48f site away and place it into a potential cage site with a certain degree of symmetry, which has possibility to form bonds with surrounding atoms and become a relative stable site for interstitial oxygen anions after geometry optimization. Since the limited symmetry of conventional cells of $La_2Hf_2O_7$, there only exist several reasonable sites can satisfy the requirements.

The formation energies of a-Fr pair defects at different positions have been computed through the difference of energy between the relaxed defect structure with oxygen migrations and the optimized original conventional cell. Oxygen atoms at 48f sites have more tendencies to escape from the original positions since oxygen atoms at 8b sites are bonded with 4 nearby La atoms with higher energy barrier. By constructing different models of 48f site oxygen atoms migration at different symmetric environment and moving distances, calculation results reflects that three types of characteristic migration paths as shown in Figure 5-7. The corresponding average defect formation energies are shown in Table 2. In the following sections, we will discuss a-Fr pair defects with each type of migration sites.

Figure 5a shows the first type of featured position for oxygen migration, locating on the vacant 8a site, which is the centre of the Hf-tetrahedral. At this site, the interstitial oxygen anions would form Hf-O bonds with the nearest 4 Hf atoms and become a 4-fold site. This site shows good symmetry and maintains good stability after geometry optimization without causing distortion on the nearby crystal structure. Regardless of the moving distance, the formation energy of this of defect site has been found to maintain close around 3.49 eV/pair. The lowest defect formation energy indicates that this site is a most stable position to incorporate the oxygen atom in the lattice. Among all migration paths, vacant 8a sites is the most favourable site for interstitial oxygen anions, which is similar with work of Djik *et al.*[29] on $Gd_2Zr_2O_7$. Figure 5b shows the partial density of states (PDOS) of $La_2Hf_2O_7$ with a-Fr pair defect of type 1. It can be seen that O-2p bands dominate the valence bands and partially unoccupied Hf-5d with empty La-4f bands dominate the conduction band. The PDOS pattern is similar with the PDOS of original conventional cell, which can be attributed to the stable lattice structure without distortion after a-Fr pair defect formed. Between O-2p and Hf-5d bands, a pair of symmetric gap states lying 1.2 eV below CBM which is mainly from hybridized O-2p and Hf-5d orbitals. Such states are actually the deep localized hole levels, which is caused by the interstitial oxygen anions in vacant 8a site.

The second type of site is a 3-fold site near the face of La-tetrahedral in the conventional cell (shown in Figure 6a). At this position, the interstitial oxygen atom will be placed to form La-O bond with the three La atoms on one face and become a distorted tetrahedral. After geometry optimization, the position of oxygen atom will adjust slightly to stable the distorted tetrahedral with equivalent bond length of three La-O bonds. Due to the repel force between two oxygen atoms, the interstitial oxygen anions might cause little deviation on the position nearest 8b site. At this site, the defect formation is all around about 6.53 eV that can be considered as a transition site between the highest and the lowest defect formation energy. Several special models prove the possibility of three-fold coordinated O atom switch between 3La atoms and 2La1Hf atoms due to their close position and formation energy. Figure 6b shows the PDOS of $La_2Hf_2O_7$ with a-Fr pair defect of type

2. Both CBM and VBM decrease and two pair of asymmetric gap states appear. O-2p mainly contributes to the two alpha states and one beta state near VBM. The other beta gap state mainly locates on 5d which may come from the Hf atom near the interstitial oxygen anion. The type 2 a-Fr defect pair induces three localized electronic levels with positions of E_V-5.0 eV, E_V+0.2 eV, and E_V+2.8 eV respectively (E_V denotes the level of valence band maximum, VBM). Those two localized electronic levels near the valence band (VB) are contributed by the p-orbitals of interstitial O ion in the lattice, while the deep electronic level is localized by the O vacancy site with hybridized *s-p-d* orbitals. Meanwhile, another two localized hole states are also induced by the type 1 a-Fr defect in the host lattice. One is staying at E_V+3.6 eV given from the p-orbital and the other is at E_V+4.6 eV by d-orbital component.

The last type of stable site is found near the 48f site that is a plane quadrangle composing by 2 oxygen atoms at 48f site and 2 La atoms. At this site, we place the interstitial oxygen anion in the centre of the plane with formation of O-O divalent bond. At this position, two different situations happened depends on the migration distance of oxygen anions. When the interstitial oxygen atom is close to the oxygen vacancy with distance below 4 Å, the interstitial oxygen has strong tendency to rebind back to the oxygen vacancy after geometry optimization. This situation can be considered as the unit cell recover to perfect cell without any defects and therefore the calculated defect energy is consistent with the optimized unit cell. As the migration distance increases, the tendency decreases and the O-O divalent bond will remain unchanged and push the nearest oxygen atom of 48f site at same plane away from its original position after optimization (shown in Figure 7a). Based on the unstable structure with O-O divalent bond, highest average defect energy has been calculated as 8.45 eV. Figure 6b shows the PDOS of $La_2Hf_2O_7$ with a-Fr pair defect of type 3. There are four spin-paired localized electronic induced in the host lattice, which are E_V-6.2 eV, E_V-5.4 eV, E_V+0.3 eV and E_V+3.3 eV, respectively. The one staying at E_V+3.3 eV is a deep donor trap level with *s-p-d* hybridized. There is also a spin-paired localized hole states near the bottom of the CBM with position of E_V+5.1 eV. Such localized hole state is dominantly hybridized by O-2p and Hf-5d orbitals with partial portion of La-4f empty states. Because of the existence of the strong O-O peroxide bond, both gap states containing p-orbital component can be attributed to the interstitial O-2p orbitals.

Based on all the simulation models, the convention cell is highly possible to recover to original condition without defect when the migration distance is less than 4 Å. After analysing quantities of models and corresponded defect formation energy, we can classify the defect formation energy into three main types with associated defect structure after geometry optimization. In each type of the defect structure, the defect formation energy shows good consistency with energy difference less than 0.7 eV. The first defect kind is forming 4-coordinated bonds in centre of the Hf-tetrahedral with average defect formation energy of 3.49 eV and Hf-O bond-length of 2.19 Å. This site shows strong stability and unity without any distortion on surrounding structure around the whole lattice. The second type of defect structure is forming 3-coordinated bonds with three metal atoms (3La atoms or 2Hf atoms with 1La atom) with average formation energy of 6.53 eV. In some of our models, these two situations can transfer to each other due to similar formation energy and close location. The last type is forming O-O divalent bond after geometry optimization, reflecting higher defect formation energy around 8.45 eV. Since this defect remain similar formation energy regardless of surrounding structure, the unstable O-O divalent bond will be responsible for higher energy.

By analysing these defect structure results from the interstitial oxygen atom, we find out that these types of sites share close locations in the lattice, which gives us some inspiration. We consider that all three types of sites can link to each other and form a relatively continuous diffuse channel for interstitial oxygen anions to keep migrating through the lattice. Figure 8 represents the proposed migration process of oxygen anions detaching from 48f site to 8a sites and Figure 9a represents the

proposed continuous migration paths between 8a-8a sites after interstitial oxygen formed a-Fr pair defect.

In Figure 8, the oxygen atom will firstly escape from the 48f site after absorbing enough energy. Then the interstitial oxygen anion has strong potential to move to closest stable vacant 8a site. At this position, the interstitial oxygen atom might move back to original position or keep moving to the second type of site that depends on the distances. When the oxygen atoms arrive at the second type of migration site, the oxygen anions can form 3-coordinated bonds. If the oxygen atom processes higher energy from lattice relaxation, it can migrate to the type 3 migration site that needs the highest energy.

From Figure 9a, we can clearly observe a continuous migration path composing the three types of defect sites we found for interstitial oxygen anions. Step 1 and Step 7 are the migration sites type 1 and Step 4 is the migration site type 3. Step 2, Step 3, Step 5 and Step 6 are migration site type 2, in which Step 3 and Step 5 form 3-fold bonds with 3 La atoms while Step 2 and Step 6 form another kind 3-fold bonds with 2Hf atoms and 1 La atoms. Figure 9b is the diagram of corresponding average formation energies of each step in reference of separation paths of 8a-8a site. The diagram shows that the distance between each step is less than 3 Å and the largest formation energy difference between a-Fr defect sites is less than 5 eV. Consequently, the interstitial oxygen atom has high possibility to vibrate from one defect site to another. The transition defects sites between vacant 8a sites can significantly decrease the barrier of oxygen diffusion. In addition, some degree of disorder in the structure can benefit both the defect formation and oxygen anions diffusion. Combining the low formation energies and continuous migration paths, we propose that the a-Fr pair defects should be the dominant source of oxygen ion conduction in $La_2Hf_2O_7$.

With analysis of energetics of the evolution behaviour of a-Fr in $La_2Hf_2O_7$ lattice, we can schematically summarize the relationship between the force F(r) and total system energy E(r) for the interstitial O ion given by the a-Fr pair defects, as shown in Figure 9 (c) and (d). From the O ion conduction path, we illustrate above (Figure 9 (a) and (b)), the total system formation energy is nearly in linear relationship with a turning point at the energy peak. The force F(r) that drives the O ion transporting presents periodic square variation behaviour in Figure 9 (c). Moreover, in pyrochlore type lattice, the O ion conduction paths gives the system with an energetic behaviour in triangle wave like function as shown in Figure 9 (d).

As shown in Figure 10, we have summarized the total energy with related to the crossover distance for the a-Fr pair defects in the host lattice, and different local bonding environment for the O-interstitial has been considered and demonstrated. The averaged minimum activation energy barrier for the O related a-Fr transporting in the host lattice is found to be 1.5 eV per pair defect, which means about 0.75 eV per defect site for generating such point defect under the lattice relaxations.

Oxygen Interstitial

Interstitial oxygen defect means an extra oxygen atom occupies an interstitial site in lattice. To compare oxygen a-Fr pair defects with other anion defects in in the pyrochlore structure, we also investigate the formation of oxygen interstitial defect in $La_2Hf_2O_7$. By putting an extra oxygen atom in the three types of defect sites that found in $La_2Hf_2O_7$, we can construct models of oxygen interstitial of $La_2Hf_2O_7$ to operate geometry optimization. The relaxed structures of interstitial oxygen defects at different defect sites are shown in Figure 11 and the corresponding formation energies are shown in Table 2.

For the relaxed structure after geometry optimization, the oxygen interstitial defects show similar behaviours as a-Fr pair defects. For defect site of type 1, the interstitial oxygen atom would also

form Hf-O bonds in the centre of Hf-tetrahedral with the 4 nearest Hf atoms and the surrounding environment is relative stable without distortion. For defect site of type 2, the oxygen interstitial was set near the face of La-tetrahedral and would form three La-O bonds. After geometry optimization, the position of oxygen interstitial slightly altered due to adjustment on La-O bond length. For defect site of type 3, the interstitial oxygen anion with O-O divalent bond will move towards the nearest 48f site after geometry optimization. The oxygen atom of nearest 48f site will be forced to move away from its original position and further cause distortion of related Hf-O bonds.

As the formation energy of oxygen interstitial are shown in Table 2, the oxygen interstitial in all three types of defect sites have close formation energies of 5.81 eV, 6.12 eV and 6.27 eV per site, respectively, which is completely different with a-Fr pair defect. The formation energies of a-Fr pair defect/site are also shown in Table 2 and compare with formation energies per site of oxygen interstitials, the highest formation energy of a-Fr defect pair at defect site type 3 still shows 2 eV lower than the lowest formation energy of interstitial defects. Based on the large formation energies difference, we can illustrate that a-Fr defect pairs have substantial priority than other anion defects on formation in pyrochlore structure. Therefore, the high performance of ion conduction in SOFCs could be ascribed to the lattice disorder caused by a-Fr pair defect.

Conclusion

In summary, we have investigated the electronic structure of $La_2Hf_2O_7$ based on first-principle calculations with particular focus on the a-Fr defect pair in terms of defect structures with correlated formation energies. The partially ordered pyrochlore structure has showed higher ion conductivity than complete ordered pyrochlore, which can be realized through the formation of a-Fr pair defects. Three types of possible migration sites have been found in the lattice that are capable to stabilize the interstitial oxygen anions escaping from 48f sites and form a-Fr pair defects. The vacant 8a site, centre of the Hf-tetrahedral, is the most possible migration site with very low average formation energy of 3.49 eV/pair. At this site, the whole lattice structure shows excellent stability with enough space to incorporate interstitial oxygen anions, which also can be proved through the basically unchanged PDOS pattern. At type 2 migration site, oxygen anion will form 3-fold bonds with 3La atoms or 2Hf and 1La atom with average formation energy of 6.53 eV/pair. A-Fr defect pair at type 3 migration site has highest cost on formation of 8.49 eV/pair that can be attributed to the formation of unstable O=O bond with highly distorted surrounding environment. Therefore, we proposed an "energy selection channel" that oxygen anions will detach from 48f site and migrate continuously between 8a sites with the assistance of type 2 and type 3 migration sites we found in the structure. These two novel sites (type 2 and type 3) are reported for first time and they are significant in constructing a migration channel for interstitial oxygen atoms. The formation of a-Fr defect pair can give higher possibilities of different "energy selection channel", which can increase the concentration of mobile oxygen anions and further explain the reason of their excellent ion conductivity. Moreover, the oxygen interstitial defects are also investigated in this work, which show much higher formation energy than a-Fr pair defect. Through this work, we propose a detailed understanding of relationship between a-Fr defect pair and electronic properties, which can further supply assistance for us to investigate other pyrochlore-type materials.

Acknowledgement

The author BH gratefully acknowledges the support of the Natural Science Foundation of China (NSFC) for the Youth Scientist grant (Grant No.: NSFC 11504309), the initial start-up grant support from the Department General Research Fund (Dept. GRF) from ABCT in the Hong Kong Polytechnic University (PolyU), and the Early Career Scheme (ECS) fund (Grant No.: PolyU

253026/16P) from the Research Grant Council (RGC) in Hong Kong. This work is supported by the high performance supercomputer (ATOM-project) in Dept. of ABCT of PolyU.

Table 1. Calculated structural $La_2Hf_2O_7$ parameters comparing with available experimental and theoretical values

Compound	a_0(Å)	dLa-O_{8b}	dLa-O_{48f}	dHf-O_{48f}
$La_2Hf_2O_7$ (GGA)	11.105	2.404	2.689	2.176
$La_2Hf_2O_7$ (GGA+U_{scf})	10.868	2.353	2.665	2.109
Ref 13	10.776	2.333	2.555	2.147
Ref 8	10.750	/	2.554	2.090
Ref 14	10.910	2.360	2.630	2.150

Table 2. The calculated average formation energies (eV/pair) of different anion defect in $La_2Hf_2O_7$.

Disorder	**A-Fr defect Formation Energy (eV/pair)**	**A-Fr defect Formation Energy (eV/site)**	**Oxygen Interstitial Defect Formation Energy (eV/site)**
Type 1	3.49	1.75	5.81
Type 2	6.53	3.27	6.12
Type 3	8.45	4.23	6.27

Figure 1.

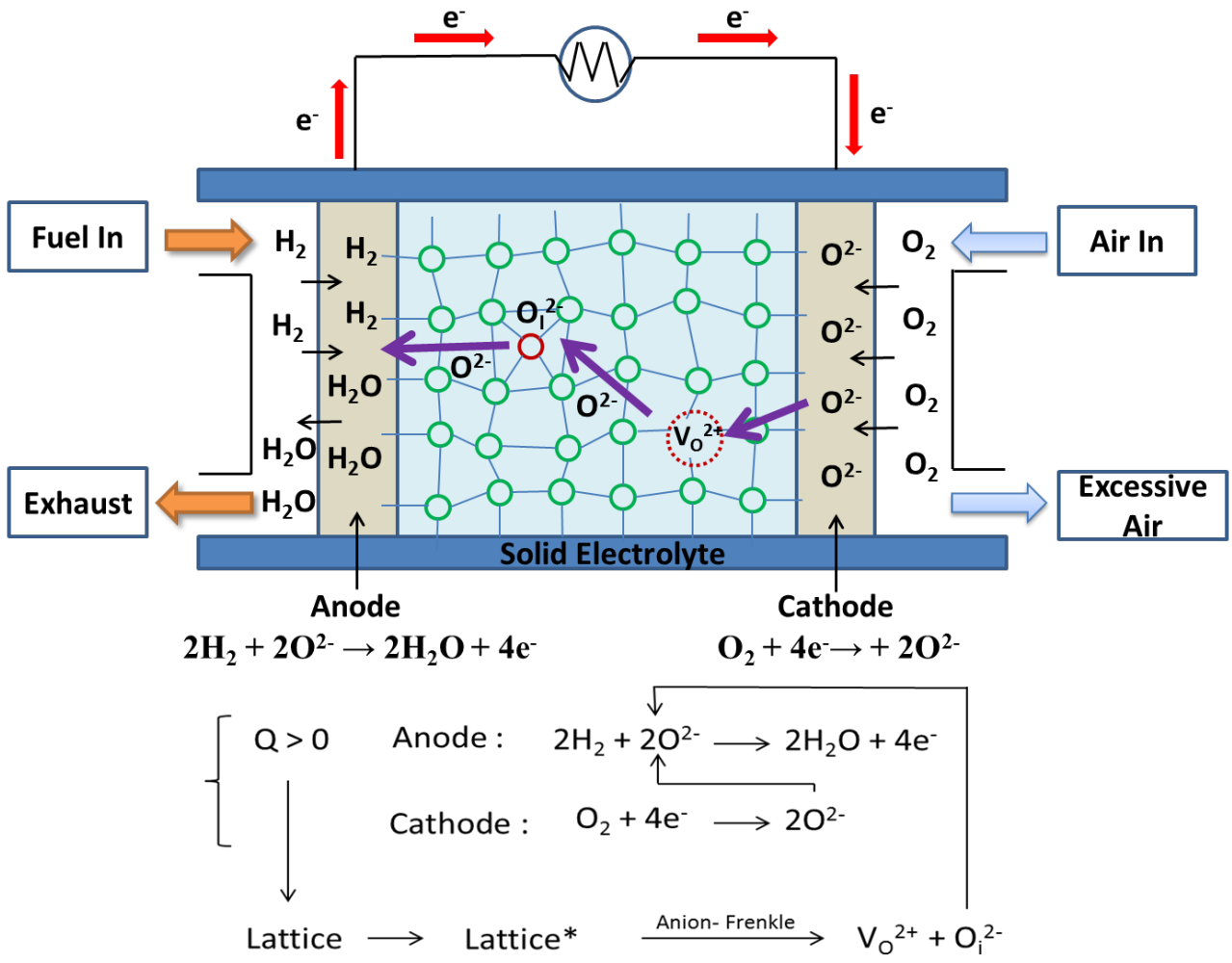

Figure 1. Concept diagram of SOFC operation based on oxygen-ion conduction

Figure 2.

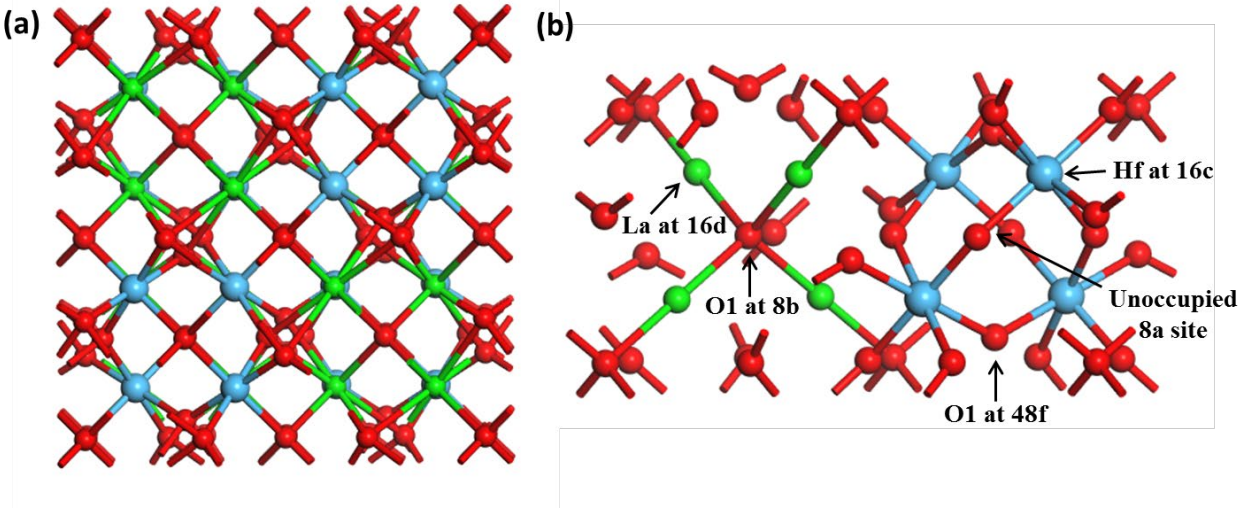

Figure 2. (a) Local view of relaxed structure of pyrochlore $La_2Hf_2O_7$ without defect (b) local structure of ground state relaxed $La_2Hf_2O_7$ pyrochlore lattice. (La=green, Hf=blue, and O=red)

Figure 3.

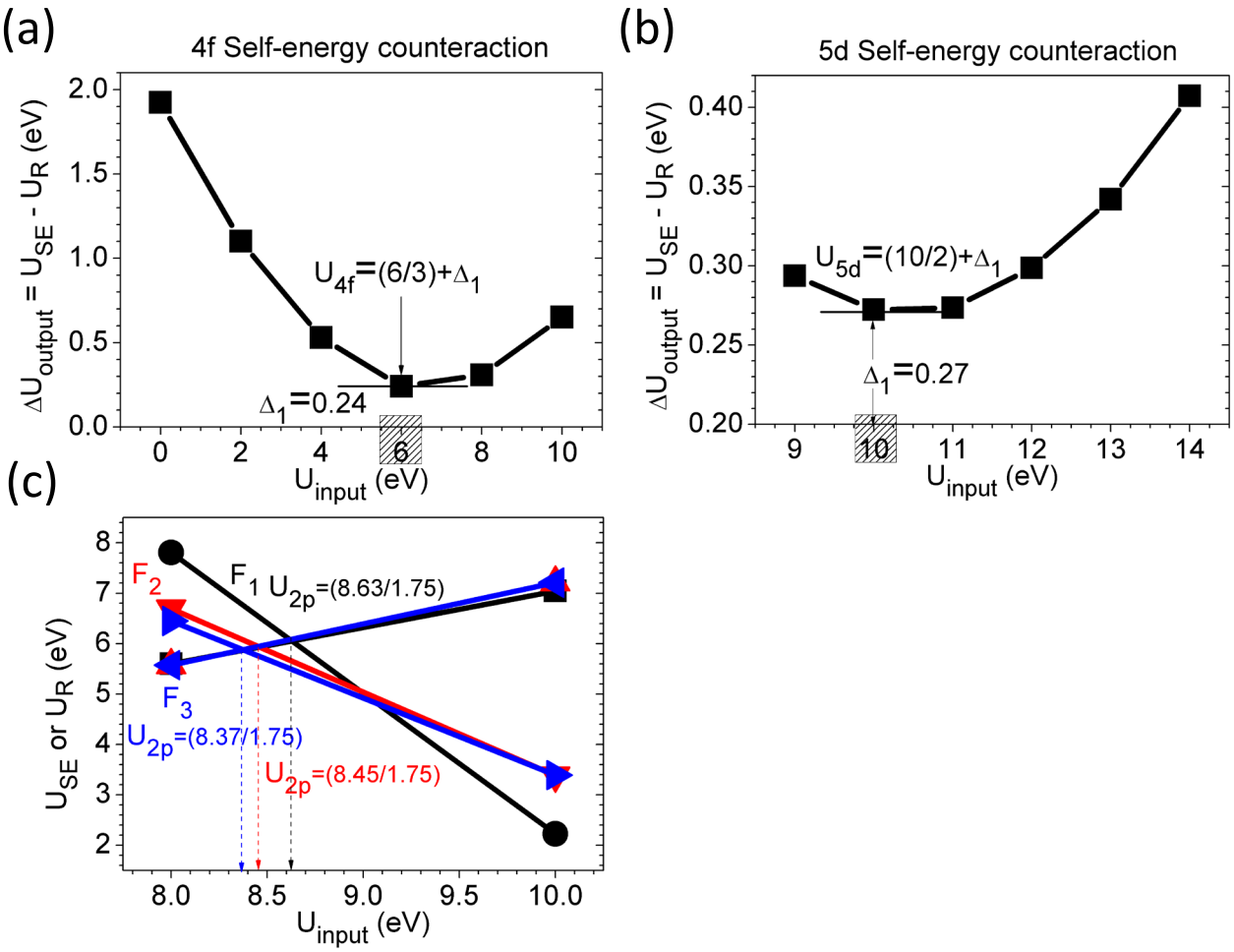

Figure 3. ab-initio determined Hubbard orbital potential correction on 4f-orbital of La sites in La2Hf2O9 (a), 5d-orbital of Hf sites (b), and the 2p of O sites (c). (Note, U_R and U_{SE} are the Hubbard projections for orbital relaxation and self-energy functionals. The Δ values in (a) and (b) are the residue when the U_R subtracted from U_{SE}. The crossover in (c) shows the self-energy is counteracted by the orbital relaxation under the perturbation in the linear response method. The U_{4f}, U_{5d}, U_{2p} are the normalized Hubbard U parameter for DFT+U calculations with minimized residue.)

Figure 4.

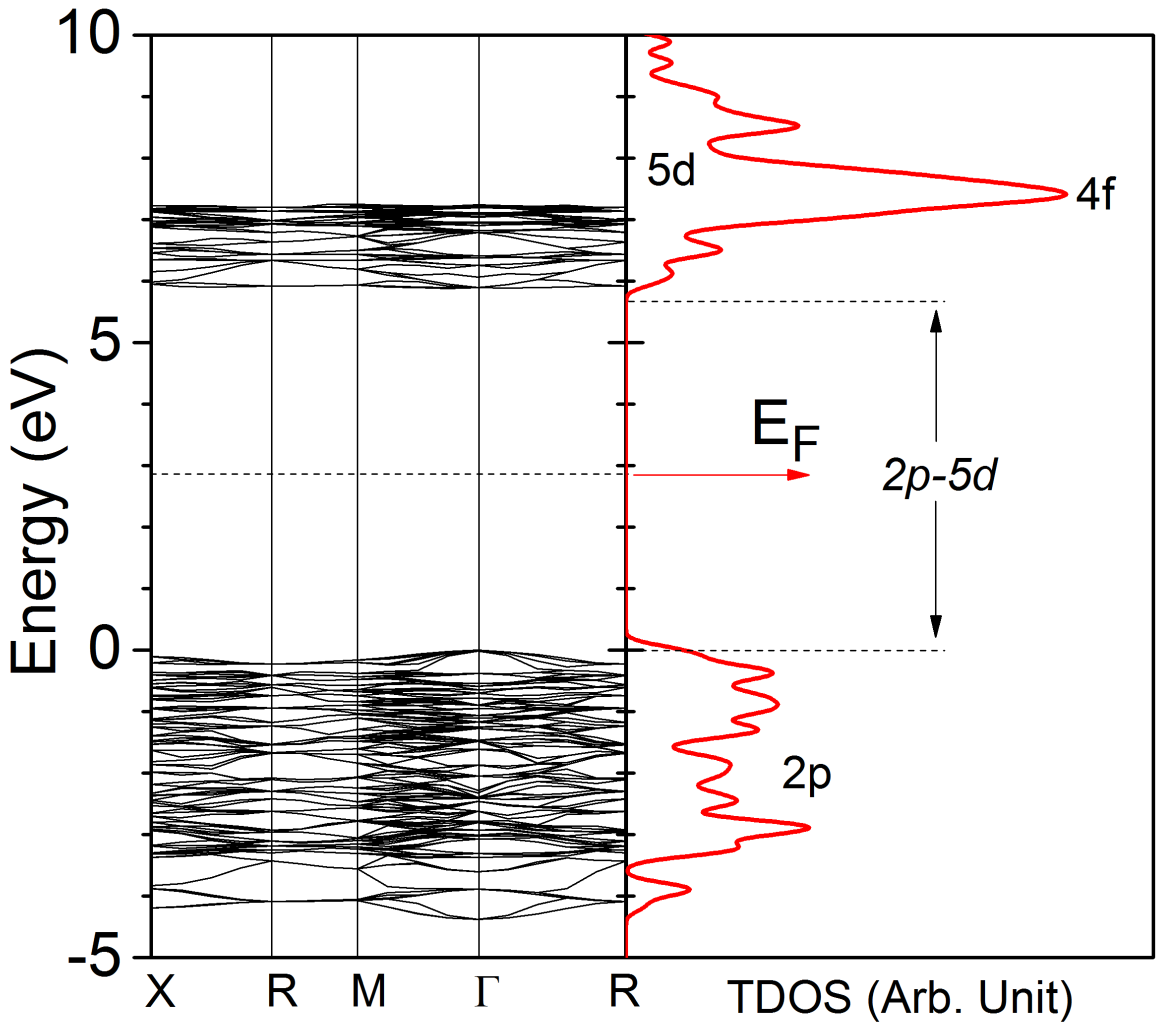

Figure 4. (Left) Calculated band structure of $La_2Hf_2O_7$. The black dash line is the Fermi level (E_F). (Right) Calculated total density of states of $La_2Hf_2O_7$ (shown as red solid line), where the bandgap is 5.880 eV. The zero energy is the highest occupied level. The red arrow is the Fermi level.

Figure 5.

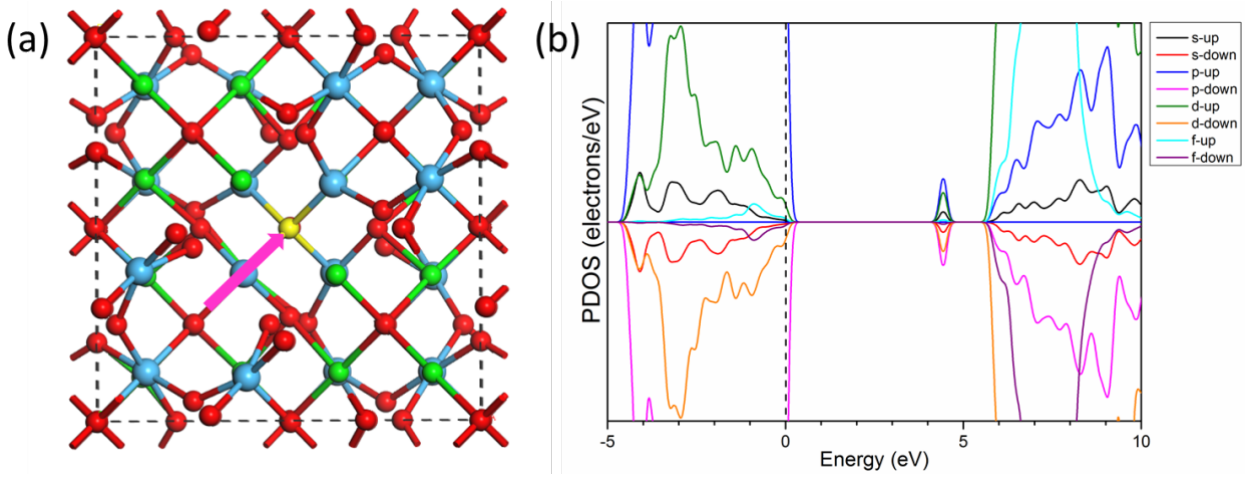

Figure 5. (a) Relaxed structure of a-Fr pair defect Type 1 in $La_2Hf_2O_7$. The pink arrow shows the formation path of the a-Fr pair defect in $La_2Hf_2O_7$. The yellow molecule represents the interstitial oxygen atom. The starting point of the arrow is the oxygen vacancy ($V_{O\,(48f)}$) site. The arrow points to the oxygen interstitial (I_O) site that located at vacant 8a site. Localized orbitals of gap states induced by the a-Fr pair defect in $La_2Hf_2O_7$. (b) Partial DOS of the a-Fr pair ($V_{O\,(48f)}$ + I_O) Type 1 in $La_2Hf_2O_7$. (La=green, Hf=blue, and O=red)

Figure 6.

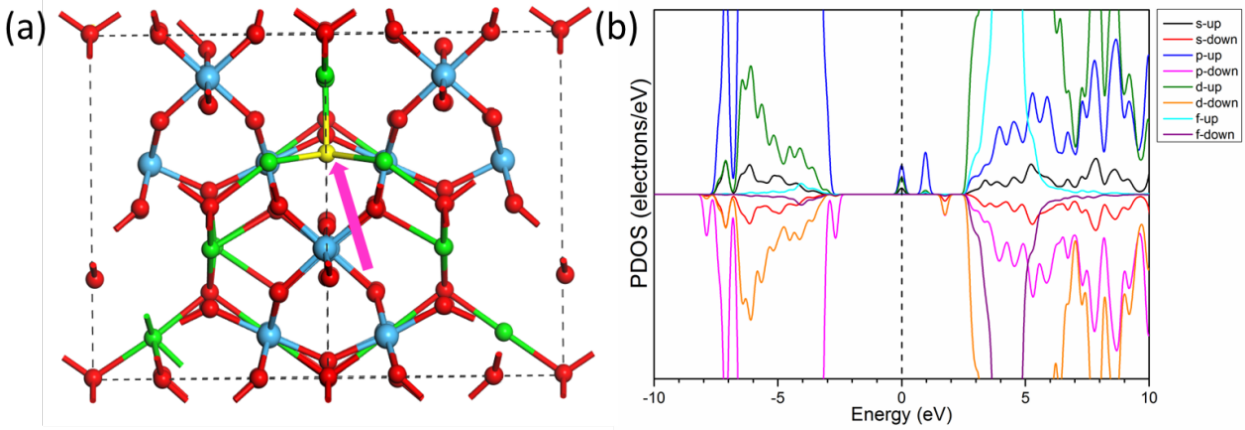

Figure 6. (a) Relaxed structure of a-Fr pair defect Type 2 in $La_2Hf_2O_7$. The pink arrow shows the formation path of the a-Fr pair defect in $La_2Hf_2O_7$. The yellow molecule represents the interstitial oxygen atom. The starting point of the arrow is the oxygen vacancy ($V_{O\,(48f)}$) site. The arrow points to the oxygen interstitial (I_O) site that located near face of the La-tetrahedral. Localized orbitals of gap states induced by the a-Fr pair defect in $La_2Hf_2O_7$. (b) Partial DOS of the a-Fr pair ($V_{O\,(48f)} + I_O$) Type 2 in $La_2Hf_2O_7$. (La=green, Hf=blue, and O=red)

Figure 7.

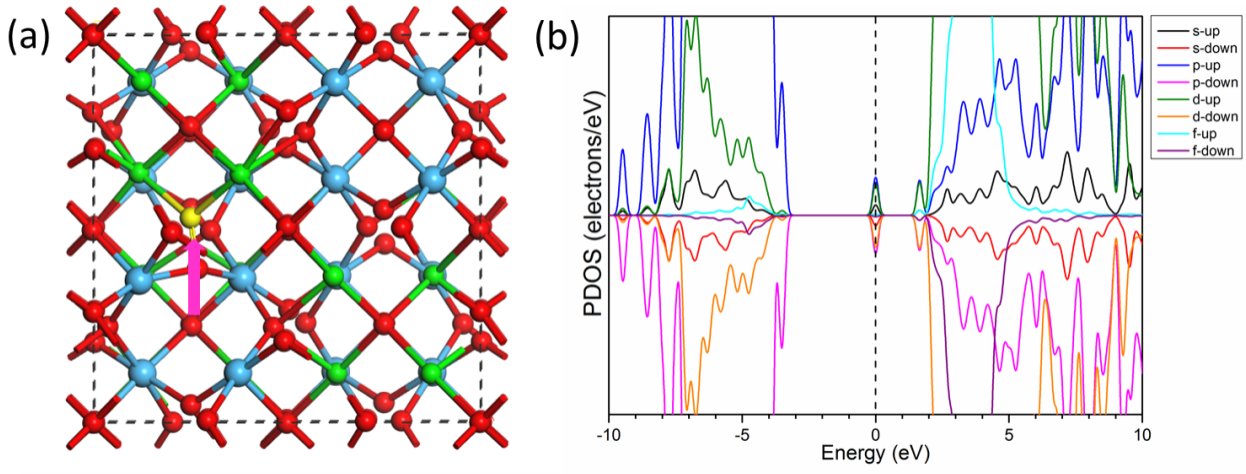

Figure 7. (a) Relaxed structure of a-Fr pair defect Type 3 in $La_2Hf_2O_7$. The pink arrow shows the formation path of the a-Fr pair defect in $La_2Hf_2O_7$. The yellow molecule represents the interstitial oxygen atom. The starting point of the arrow is the oxygen vacancy ($V_{O\,(48f)}$) site. The arrow points to the oxygen interstitial (I_O) site that located near oxygen atom at 48f. Localized orbitals of gap states induced by the a-Fr pair defect in $La_2Hf_2O_7$. (b) Partial DOS of the a-Fr pair ($V_{O\,(48f)}$ + I_O) Type 3 in $La_2Hf_2O_7$. (La=green, Hf=blue, and O=red)

Figure 8.

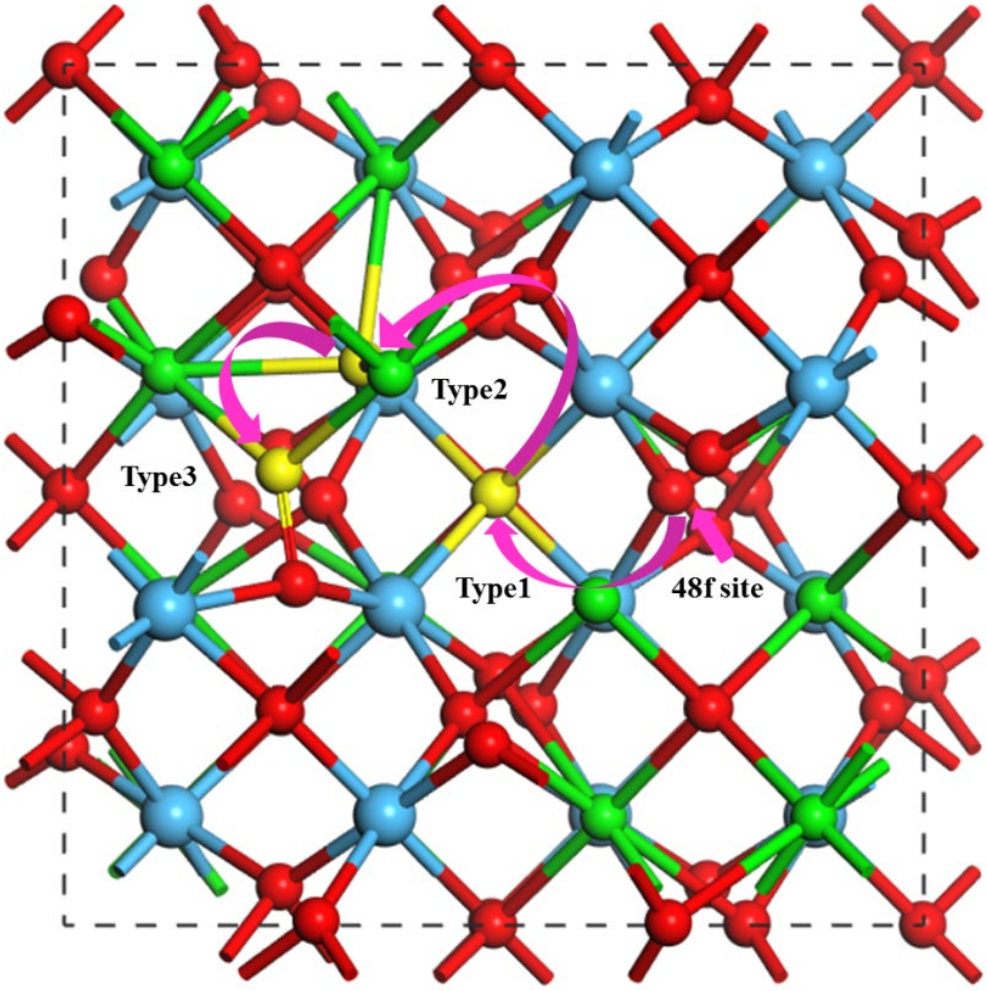

Figure 8. Diagram of constructed migration path for oxygen anions from 48f site. The pink arrows show the migration direction of oxygen anions. The yellow molecule represents the interstitial oxygen atom at each type of migration sites. Through this repeated migration path, interstitial oxygen anions can diffuse in the structure. (La=green, Hf=blue, and O=red)

Figure 9.

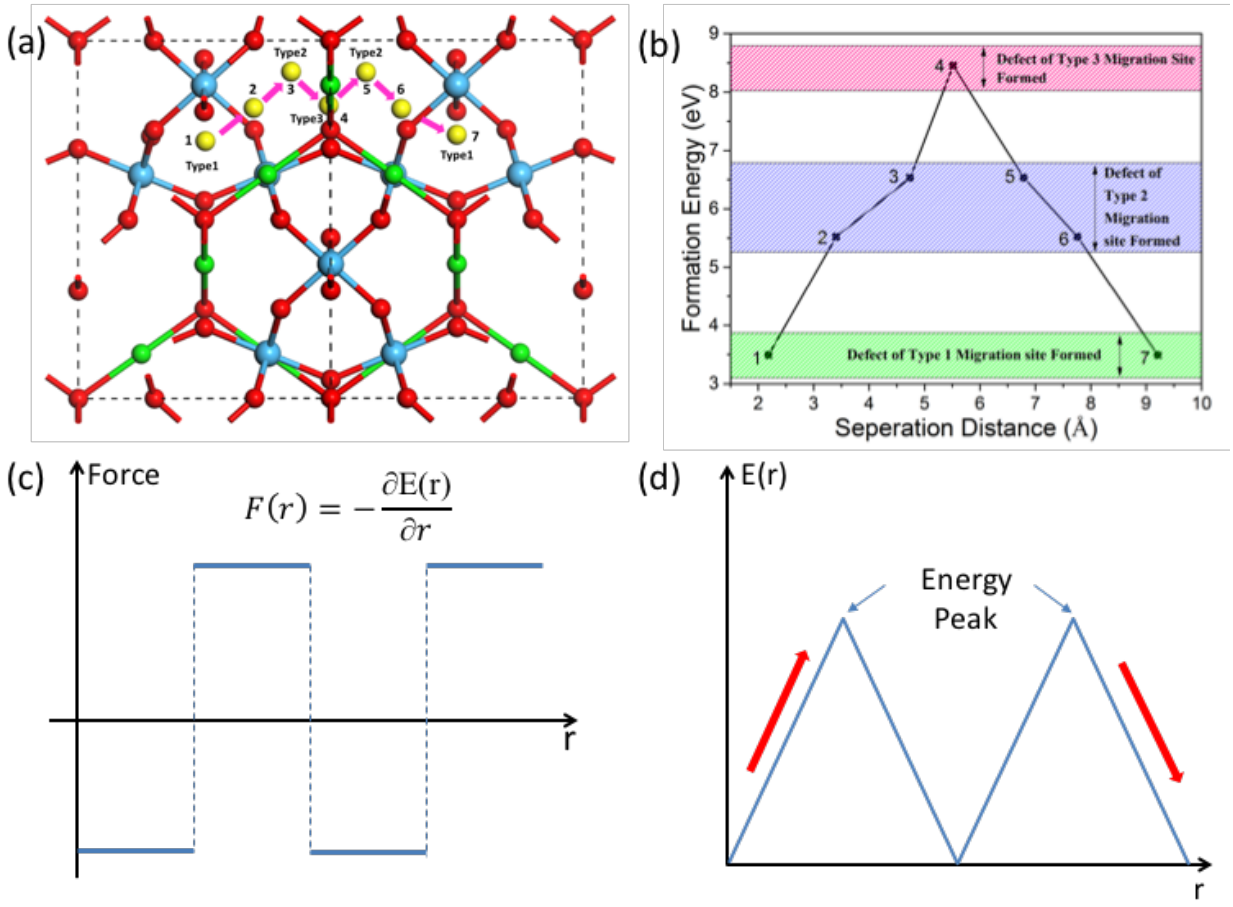

Figure 9. (a) Diagram of proposed migration path for oxygen anions between vacant 8a sites. The pink arrows show the migration direction of oxygen anions. The yellow molecule represents the interstitial oxygen atom at each type of migration sites. Through this repeated migration path, interstitial oxygen anions can diffuse in the structure. (b) The corresponding diagram of formation energies (per pair) of a-Fr pair defect with reference of separation (in angstrom) of the a-Fr pair. (c) The schematic diagram to illustrate the force F(r) that O-interstitial experienced through the host lattice given by a-Fr pair defects along the proposed path. (d) The related total energy in the system induced by the a-Fr pair defect transporting through the lattice along the path. (La=green, Hf=blue, and O=red)

Figure 10.

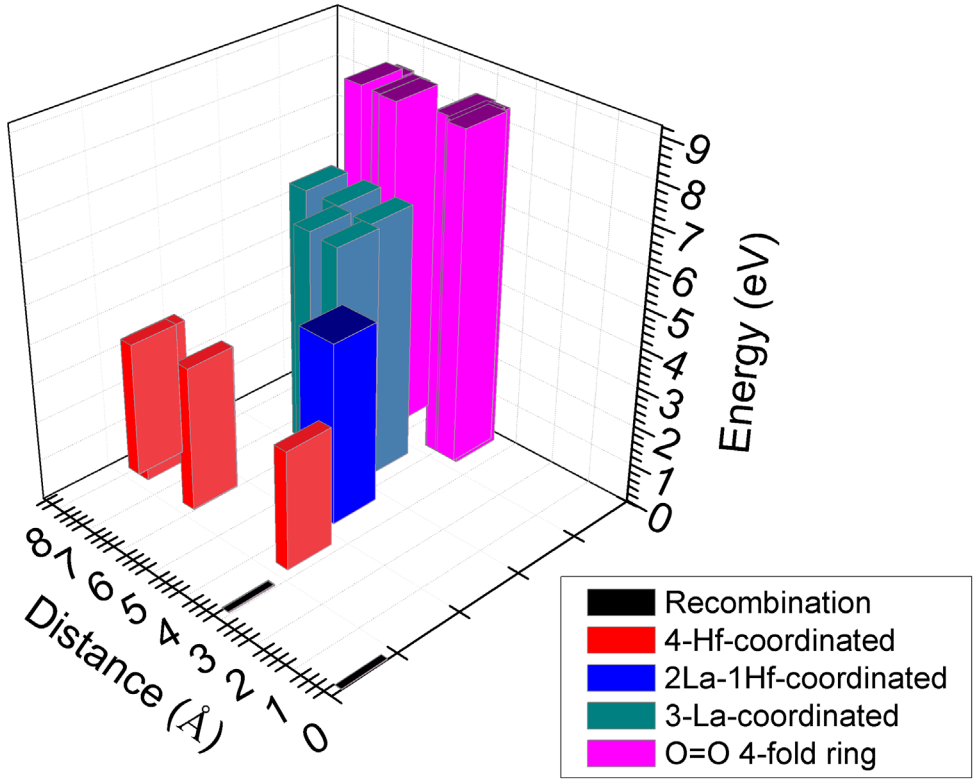

Figure 10. Summary of the total energy with related to the crossover distance for the a-Fr pair defects within various local bonding environments

Figure 11.

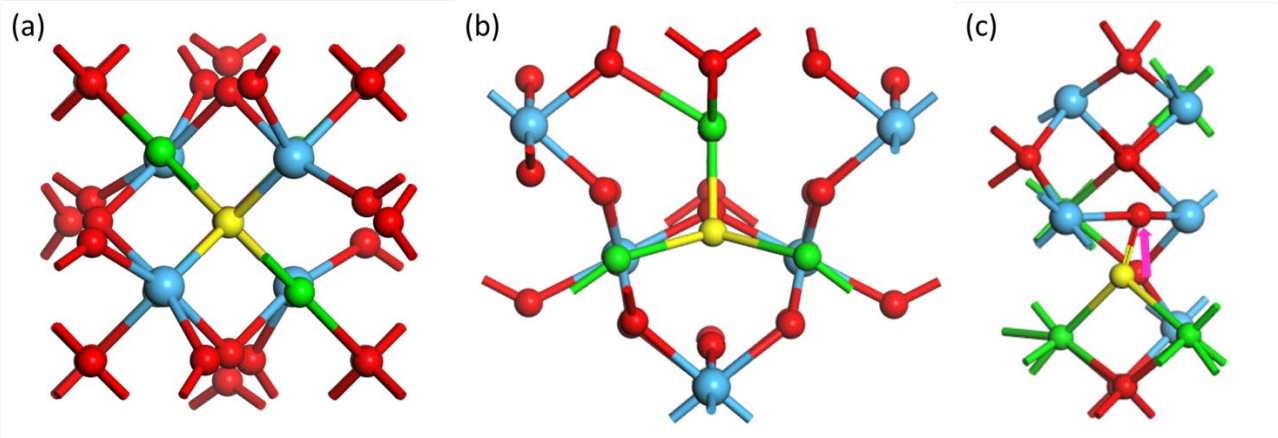

Figure 11. Relaxed structure of interstitial oxygen at different defect sites in $La_2Hf_2O_7$. The yellow molecule represents the interstitial oxygen atom. (a) Relaxed structure of interstitial oxygen at defect site Type 1. The surrounding structure remains unchanged after relaxation. (b) Relaxed structure of interstitial oxygen at defect site Type 2. The surrounding structure remains unchanged after relaxation. (c) Relaxed structure of interstitial oxygen at defect site Type 3. The pink arrow shows the direction of distortion of surrounding structure after relaxation. (La=green, Hf=blue, and O=red)

References

(1) Minh, N. Solid oxide fuel cell technology-features and applications. *Solid State Ionics* **2004,** *174* (1-4), 271.

(2) Singhal, S. Advances in solid oxide fuel cell technology. *Solid State Ionics* **2000,** *135* (1-4), 305.

(3) Stambouli, A. B.; Traversa, E. Solid oxide fuel cells (SOFCs): a review of an environmentally clean and efficient source of energy. *Renewable and Sustainable Energy Reviews* **2002,** *6* (5), 433.

(4) Minh, N. Q. Ceramic fuel cells. *J. Am. Ceram. Soc.* **1993,** *76* (3), 563.

(5) Dixon, J. M.; LaGrange, L. D.; Merten, U.; Miller, C. F.; Porter, J. T. Electrical resistivity of stabilized zirconia at elevated temperatures. *J. Electrochem. Soc.* **1963,** *110* (4), 276.

(6) Nomura, K. Aging and raman scattering study of scandia and yttria doped zirconia. *Solid State Ionics* **2000,** *132* (3-4), 235.

(7) Tsoga, A.; Gupta, A.; Naoumidis, A.; Nikolopoulos, P. Gadolinia-doped ceria and yttria stabilized zirconia interfaces: regarding their application for SOFC technology. *Acta Mater.* **2000,** *48* (18-19), 4709.

(8) Anderson, M. D.; Stevenson, J. W.; Simner, S. P. Reactivity of lanthanide ferrite SOFC cathodes with YSZ electrolyte. *J. Power Sources* **2004,** *129* (2), 188.

(9) Knell, A. CO oxidation over Au/ZrO_2 catalysts: Activity, deactivation behavior, and reaction mechanism. *J. Catal.* **1992,** *137* (2), 306.

(10) Tomishige, K.; Furusawa, Y.; Ikeda, Y.; Asadullah, M.; Fujimoto, K. CeO_2–ZrO_2 solid solution catalyst for selective synthesis of dimethyl carbonate from methanol and carbon dioxide. *Catal. Lett.* **2001,** *76* (1/2), 71.

(11) Badwal, S. P. S. Yttria tetragonal zirconia polycrystalline electrolytes for solid state electrochemical cells. *Applied Physics A Solids and Surfaces* **1990,** *50* (5), 449.

(12) Houssa, M.; Afanas'ev, V. V.; Stesmans, A.; Heyns, M. M. Variation in the fixed charge density of SiO_x/ZrO_2 gate dielectric stacks during postdeposition oxidation. *Appl. Phys. Lett.* **2000,** *77* (12), 1885.

(13) Slifka, A. J.; Filla, B. J.; Phelps, J. M.; Bancke, G.; Berndt, C. C. Thermal conductivity of a zirconia thermal barrier coating. *J. Therm. Spray Technol.* **1998,** *7* (1), 43.

(14) Yuan, Q.; Liu, Q.; Song, W. G.; Feng, W.; Pu, W. L.; Sun, L. D.; Zhang, Y. W.; Yan, C. H. Ordered mesoporous $Ce_{1-x}Zr_xO_2$ solid solutions with crystalline walls. *J. Am. Chem. Soc.* **2007,** *129* (21), 6698.

(15) Yuan, Q.; Li, L.-L.; Lu, S.-L.; Duan, H.-H.; Li, Z.-X.; Zhu, Y.-X.; Yan, C.-H. Facile synthesis of zr-based functional materials with highly ordered mesoporous structures. *The Journal of Physical Chemistry C* **2009,** *113* (10), 4117.

(16) Solomon, S.; George, A.; Thomas, J. K.; John, A. Preparation, characterization, and ionic transport properties of nanoscale $Ln_2Zr_2O_7$ (Ln = Ce, Pr, Nd, Sm, Gd, Dy, Er, and Yb) energy materials. *J. Electron. Mater.* **2014,** *44* (1), 28.

(17) Hao, C. K.; Lee, C. S. Metal-doped pyrochlore as novel electrode materials for intermediate temperature solid oxide fuel cell. *ECS Transactions* **2013,** *58* (3), 165.

(18) Yamamura, H.; Nishinoa, H.; Kakinumaa, K.; Nomurab, K. Electrical conductivity anomaly around fluorite–pyrochlore phase boundary. *Solid State Ionics* **2003,** *158* (3-4), 359.

(19) Blanchard, P. E. R.; Liu, S.; Kennedy, B. J.; Ling, C. D.; Avdeev, M.; Aitken, J. B.; Cowie, B. C. C.; Tadich, A. Investigating the local structure of lanthanoid hafnates $Ln_2Zr_2O_7$ via diffraction and spectroscopy. *The Journal of Physical Chemistry C* **2013,** *117* (5), 2266.

(20) Karthik, C.; Anderson, T. J.; Gout, D.; Ubic, R. Transmission electron microscopic study of pyrochlore to defect-fluorite transition in rare-earth pyrohafnates. *Journal of Solid State Chemistry* **2012,** *194*, 168.

(21) Lehmann, H.; Pitzer, D.; Pracht, G.; Vassen, R.; Stöver, D. Thermal conductivity and thermal expansion coefficients of the lanthanum rare-earth-element zirconate system. *Journal of the American Ceramic Society* **2003,** *86* (8), 1338.

(22) Eagleman, Y.; Weber, M.; Chaudhry, A.; Derenzo, S. Luminescence study of cerium-doped $La_2Zr_2O_7$: Effects due to trivalent and tetravalent cerium and oxygen vacancies. *Journal of Luminescence* **2012,** *132* (11), 2889.

(23) Ji, Y.; Jiang, D.; Shi, J. $La_2Hf_2O_7$: Ti^{4+} ceramic scintillator for x-ray imaging. *J. Mater. Res.* **2011,** *20* (03), 567.

(24) Wei, F.; Tu, H.; Wang, Y.; Yue, S.; Du, J. Epitaxy growth and electrical properties of $La_2Hf_2O_7$ thin film on Si (001) substrate by pulsed laser deposition. *Journal of Physics: Conference Series* **2009,** *152*, 012003.
(25) Seguini, G.; Spiga, S.; Bonera, E.; Fanciulli, M.; Reyes Huamantinco, A.; Först, C. J.; Ashman, C. R.; Blöchl, P. E.; Dimoulas, A.; Mavrou, G. Band alignment at the $La_2Hf_2O_7$/(001) Si interface. *Appl. Phys. Lett.* **2006,** *88* (20), 202903.
(26) Lumpkin, G. R.; Whittle, K. R.; Rios, S.; Smith, K. L.; Zaluzec, N. J. Temperature dependence of ion irradiation damage in the pyrochlores $La_2Zr_2O_7$ and $La_2Hf_2O_7$. *J. Phys.: Condens. Matter* **2004,** *16* (47), 8557.
(27) Ewing, R. C.; Weber, W. J.; Lian, J. Nuclear waste disposal—pyrochlore ($A_2B_2O_7$): Nuclear waste form for the immobilization of plutonium and "minor" actinides. *J. Appl. Phys.* **2004,** *95* (11), 5949.
(28) Burggraaf, A.; Vandijk, T.; Verkerk, M. Structure and conductivity of pyrochlore and fluorite type solid solutions. *Solid State Ionics* **1981,** *5*, 519.
(29) Vandijk, M.; Burggraaf, A.; Cormack, A.; Catlow, C. Defect structures and migration mechanisms in oxide pyrochlores. *Solid State Ionics* **1985,** *17* (2), 159.
(30) Minervini, L.; Grimes, R. W.; Sickafus, K. E. Disorder in pyrochlore oxides. *J. Am. Ceram. Soc.* **2004,** *83* (8), 1873.
(31) Hagiwara, T.; Yamamura, H.; Nishino, H. Relationship between oxide-ion conductivity and ordering of oxygen vacancy in the $La_2Zr_2O_7$ (Ln= La, Nd, Eu) system having a pyrochlore composition. *IOP Conference Series: Materials Science and Engineering* **2011,** *18* (13), 132003.
(32) Wilde, P.; Catlow, C. Defects and diffusion in pyrochlore structured oxides. *Solid State Ionics* **1998,** *112* (3-4), 173.
(33) Terki, R.; Feraoun, H.; Bertrand, G.; Aourag, H. Full potential linearized augmented plane wave investigations of structural and electronic properties of pyrochlore systems. *Journal of Applied Physics* **2004,** *96* (11), 6482.
(34) Pruneda, J. M.; Artacho, E. First-principles study of structural, elastic, and bonding properties of pyrochlores. *Physical Review B* **2005,** *72* (8).
(35) Li, N.; Xiao, H. Y.; Zu, X. T.; Wang, L. M.; Ewing, R. C.; Lian, J.; Gao, F. First-principles study of electronic properties of $La_2Hf_2O_7$ and $Gd_2Hf_2O_7$. *J. Appl. Phys.* **2007,** *102* (6), 063704.
(36) Panero, W. R.; Stixrude, L.; Ewing, R. C. First-principles calculation of defect-formation energies in the $Y_2(Ti,Sn,Zr)_2O_7$ pyrochlore. *Physical Review B* **2004,** *70* (5).
(37) Sleight, A. W. New ternary oxides of mercury with the pyrochlore structure. *Inorganic Chemistry* **1968,** *7* (9), 1704.
(38) Subramanian, M. A.; Aravamudan, G.; Subba Rao, G. V. Oxide pyrochlores — A review. *Progress in Solid State Chemistry* **1983,** *15* (2), 55.
(39) Dijk, M. P. V.; Vries, K. J. D.; Burggraaf, A. J. Study of the oxygen electrode reaction using mixed conducting oxide surface layers. Part I: Experimental methods and current-overvoltage experiments. *Solid State Ionics* **1986,** *21* (1), 73.

TOC

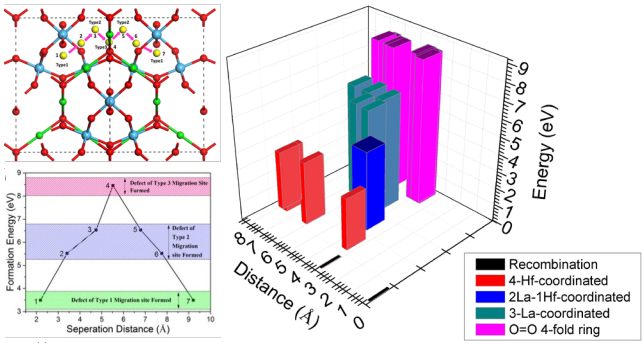

Synopsis (75 words)

The total energy with related to the crossover distance for the a-Fr pair defects in the host lattice, and different local bonding environment for the O-interstitial has been considered and demonstrated. The averaged minimum activation energy barrier for the O related a-Fr transporting in the host lattice is found to be 1.5 eV per pair defect, which means about 0.75 eV per defect site for generating such point defect under the lattice relaxations.